DIFFERENTIATION OF METAL-RICH METEORITIC PARENT BODIES. M. I. Petaev[1,2] and S. B. Jacobsen[2], [1]Harvard-Smithsonian Center for Astrophysics, 60 Garden St, Cambridge, MA 02138, USA; [2]Department of Earth and Planetary Sciences, Harvard University, 20 Oxford Street, Cambridge, MA 02139, USA. (mpetaev@cfa.harvard.edu).

Introduction: There is now increasing evidence that the timescale between the formation of CAIs and of chondrules is < 1-2 Ma, and that the achondritic parent planets may have formed and differentiated within 2-4 Ma of the origin of the Solar System [1,2]. Long-lived chronometers (such as ^{187}Re-^{187}Os) provide some broad constraints on the chronology and differentiation processes in the early Solar System. The isotopic record of extinct radionuclides (such as ^{107}Pd and ^{182}Hf), may potentially yield more reliable constraints on the rates of accretion, core formation, and the earliest evolution of the mantle and crust in planetesimals and planets. Our goal is to investigate differentiation processes and to establish reliable timescales for the early stages of planetary evolution by modeling the trace element behavior, isotopic evolution, and parent/daughter fractionations of the Re-Pt-Os, Pd-Ag, and Hf-W systems. For the purpose of this study we need high quality elemental and isotopic data on Mo, Re, Os, Pt, Pd, Ag, and W as well as reliable transport models for these elements during planetary differentiation.

There are quite a few models [3-20] which explore various aspects of the behavior of minor and trace elements during core formation as well as fractionation of siderophile elements during core crystallization. The models of core crystallization provide important information on how the chemical compositions of the magmatic iron meteorites are affected by the presence of sulfur and phosphorus in the melt [10, 16, 17], by the dendritic growth of metal crystals [11, 12], by liquid immiscibility [14, 17], by the entrapment of sulfur-rich melt [12,14,15,18], and by mixing in the partially molten core [16]. However, with a few exceptions [16, 17, 20], the suite of chemical elements modeled is usually limited to Ni, As, Ga, Ge, Ir, and Au and does not include Re, Os, Pt, Pd, Ag, and W, which are important for isotopic chronometry. As a step toward developing a comprehensive model, we describe here our new FeNiSP code and use it to interpret trace element patterns of iron meteorites and the Divnoe primitive achondrite reported in the accompanying abstract [21].

Modeling and computer code: The FeNiSP computer code is a FORTRAN program which models partitioning of Fe, Ni, S, P, Cr, Co, Ga, Ge, As, Mo, Ru, Rh, Pd, Ag, W, Re, Os, Ir, Pt, and Au between the solid and liquid phases during crystallization of a Fe-Ni-S-P-rich melt. The input parameters of the FeNiSP code include the bulk composition of the system, the range of degrees of crystallization, the increment in degrees of crystallization, the values of distribution coefficients (S,P-dependent), the mode of crystallization (F_{is}) expressed as the fraction of crystals isolated from the melt at each iteration, and the fraction of the melt trapped by growing crystals (F_{tr}). The addition of F_{is} allows us to explore, if necessary, modes of crystallization intermediate between the full equilibrium (F_{is} = 0) and the Rayleigh fractional crystallization (F_{is} = 1). When necessary, the values of distribution coefficients can be changed without changing the code.

At each step, FeNiSP calculates the equilibrium partitioning of all elements, except Fe and S, between the residual liquid and the solid metal. The concentrations of the Fe and S are calculated by mass-balancing the amounts of these elements in the system assuming that all S resides in the melt. After subtracting the appropriate portion of solid metal from the bulk composition of the core, the process continues until either the maximum crystallization degree specified or the metal-troilite eutectic is reached. The code outputs chemical compositions and the abundances of liquid and solid phases for the values of crystallization degrees specified.

In this study we used the set of distribution coefficients from Liu and Fleet [20] (except for Re and Os [17]) whose values are consistent with the results of previous investigators.

Results and conclusions: The results of model calculations for metals of the Divnoe primitive achondrite and the IIIAB irons are shown in Figs. 1 and 2. Figs. 3-7 show HSE patterns of iron meteorites measured by us [21].

Modeling the equilibrium partial melting of the Divnoe metal (5.27 wt.% Ni, 10.23 % S, 0.39 % Co, 0.05 % P [22], other elements enriched by 10×CI) shows a very good match at 62% partial melting of the current Fe-Ni-S assemblage (Fig. 1). It appears that the Divnoe metal is the residue of partial melting as is its silicate fraction [22].

Fig. 2 shows calculated HSE patterns of Fe,Ni metal formed by fractional crystallization of the core of IIIAB irons. Following [20], we used the initial S content of the IIIAB core from [23]. The calculated HSE patterns are quite similar to those in the IIIAB (Fig. 3), IIAB (Fig. 5), IVA (Fig. 6), and IVB (Fig.7) meteorites, which are believed to have formed by fractional crystallization of their source regions.

Essentially all patterns have two regions, either concave or convex, separated by Pd, which shows a very limited range of variations. The fact that the calculated range of Pd variations is considerably larger than

the measured one, suggests that the distribution coefficient of Pd [20] used in our modeling needs to be revised. Mo is another element that shows a very limited range of variations.

The HSE patterns of the IA irons, Toluca and Odessa (Fig. 4), are also curved, pointing to their formation by fractional crystallization. The HSE pattern of the IC iron, Arispe, is very similar to that of Divnoe, which suggest that Arispe is the residue of nearly equilibrium partial melting. The HSE pattern of Chinga (Fig. 7) clearly shows that this ataxite is anomalous.

The small ranges of variations in concentrations of highly siderophile Mo and Pd within individual groups make these elements suitable for estimating mass fractions of the cores in their parent bodies. For this purpose we prefer Mo to Pd because of its highly refractory behavior. Assuming that the parent bodies of iron meteorites initially contained the cosmic inventory of refractory siderophiles, one can estimate the mass fractions of their cores (~20 % for IA, IIA, IIIAB, and IVA, and ~ 6 % for IVB) from the Mo enrichment factors shown in Figs. 3-7.

References: [1]Lugmair, G.W. and Shukolyukov, A. (1998) *GCA,* 62, 2863-2886. [2] Yin Q. et al. (2002) *Nature, 418*, 949-952. [3] Richter K. and Drake M. J. (1996) *Icarus, 124*, 513-529. [4] Richter K. et al. (1997) *Phys. Earth Planet. Int., 100*, 115-134. [5] Harper C. L. and Jacobsen S. B. (1996) *GCA, 60*, 1131-1153. [6] Richter K. and Drake M. J. (1997) *EPSL, 146*, 541-553. [7] Richter K. and Drake M. J. (2000) *GCA, 64*, 3581-3597. [8] Scott E. R. D. (1972) *GCA, 36*, 1205-1236. [9] Kracher A. and Wasson J. T. (1982) *GCA, 46,* 2419-2426. [10] Jones J. H. and Drake M. J. (1983) *GCA, 47*, 1199-1209. [11] Haack H. and Scott E. R. D. (1992) *JGR, 97*, 14727-14734. [12] Haack H. and Scott E. R. D. (1993) *GCA, 57*, 3457-3472. [13] Scott E. R. D. et al. (1996) *GCA, 60*, 1615-1631. [14] Ulf-Møller F. (1999) *MAPS, 33*, 207-220. [15] Wasson J. T. (1999) *GCA, 63*, 2875–2889. [16] Chabot N. L. and Drake M. J. (1999) *MAPS, 34*, 235-246. [17] Chabot N. L. and Drake M. J. (2000) *MAPS, 35*, 807-816. [18] Wasson J. T. and Richardson J. W. (2001) *GCA, 65*, 951–970. [19] Wasson J. T. and Kallemeyn G. W. (2002) *GCA, 66*, 2445–2473. [20] Liu M. and Fleet M. E. (2001) *GCA 65*, 671-682. [21] Petaev M. I. and Jacobsen S. B. (2003) this volume. [22] Petaev M. I. et al. (1994) *Meteoritics,* 29, 182-199.

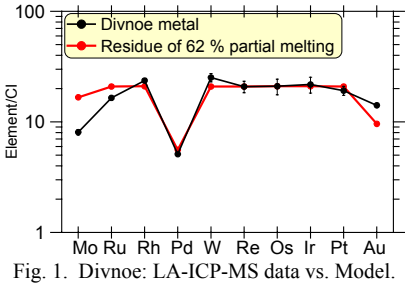

Fig. 1. Divnoe: LA-ICP-MS data vs. Model.

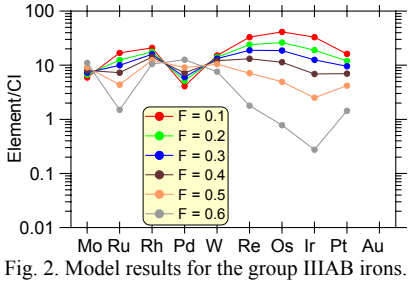

Fig. 2. Model results for the group IIIAB irons.

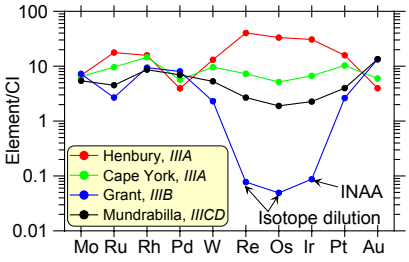

Fig. 3. Group III irons: LA-ICP-MS data.

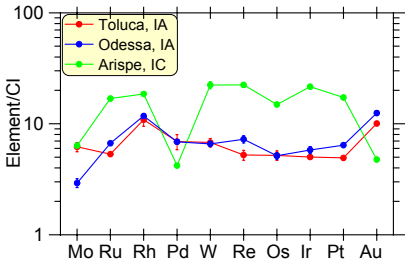

Fig. 4. Group I irons: LA-ICP-MS data.

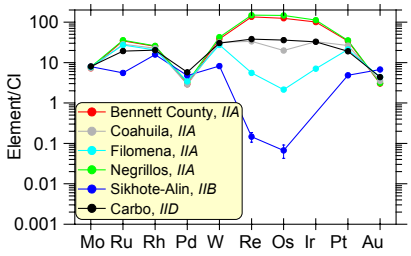

Fig. 5. Group II irons: LA-ICP-MS data.

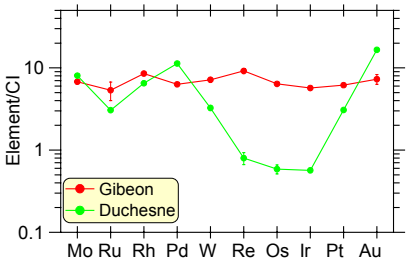

Fig. 6. Group IVA irons: LA-ICP-MS data.

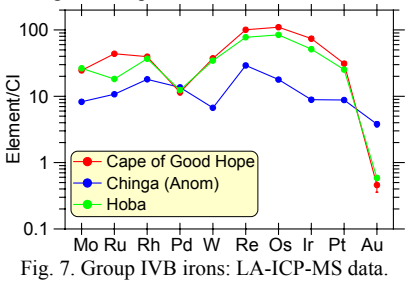

Fig. 7. Group IVB irons: LA-ICP-MS data.